manuscript No.
(will be inserted by the editor)

A Single Laser System for Ground State Cooling of $^{25}Mg^+$

Boerge Hemmerling[1], Florian Gebert[1], Yong Wan[1], Daniel Nigg[3], Ivan V. Sherstov[1], Piet O. Schmidt[1,2]

[1] QUEST Institute for Experimental Quantum Metrology, Physikalisch-Technische Bundesanstalt, Bundesallee 100, 38116 Braunschweig, Germany
e-mail: boerge.hemmerling@quantummetrology.de
[2] Institut für Quantenoptik, Leibniz Universität Hannover, Welfengarten 1, 30167 Hannover, Germany
[3] *Present address:* Institut für Experimentalphysik, Universität Innsbruck, 6020 Innsbruck, Austria

Received: date / Revised version: date

Abstract We present a single solid-state laser system to cool, coherently manipulate and detect $^{25}Mg^+$ ions. Coherent manipulation is accomplished by coupling two hyperfine ground state levels using a pair of far-detuned Raman laser beams. Resonant light for Doppler cooling and detection is derived from the same laser source by means of an electro-optic modulator, generating a sideband which is resonant with the atomic transition. We demonstrate ground-state cooling of one of the vibrational modes of the ion in the trap using resolved-sideband cooling. The cooling performance is studied and discussed by observing the temporal evolution of Raman-stimulated sideband transitions. The setup is a major simplification over existing state-of-the-art systems, typically involving up to three separate laser sources.

1 Introduction

Over the last decades, ion trap experiments have become versatile instruments to investigate a variety of physical phenomena, ranging from quantum computing [1, 2], optical clocks [3,4] and precision spectroscopy [5,6,7] to quantum simulations [8,9]. Many applications benefit from the fact that ions can be easily stored [10], with trap life times spanning from hours to months, and coherently manipulated with commercially available laser systems. Furthermore, trapped ions feature very long coherence times [11,12] and the possibility of cooling the external degrees of freedom to the vibrational ground state [13,14,15], making them an ideal testbed to investigate quantum mechanics. The strong Coulomb interaction can then be used to sympathetically cool simultaneously stored charged particles, opening new prospects for cooling of complex molecular ions to the rotational and vibrational ground state [16,17].

In many experiments, ions with hyperfine structure (e.g. $^{43}Ca^+$[18], $^9Be^+$[19], $^{111}Cd^+$[20], $^{25}Mg^+$[8], Yb^+[21]) are employed. For quantum computing experiments the long-lived hyperfine ground states are usually chosen as qubit states. Ground state cooling is achieved by driving optical Raman transitions between these states, which often requires several complex Raman and repumping laser systems [19]. Here, we report on cooling of the $^{25}Mg^+$ isotope to the vibrational ground state using a single solid-state fibre laser system with an incorporated electro-optical modulator. The presented laser setup is a major simplification to previously used state-of-the-art Mg^+ laser systems [22].

This paper is organized as follows. In Section 2 the experimental setup used for trapping, cooling and manipulating a single $^{25}Mg^+$ ion in a Paul trap is described. In Section 3 the sequences to achieve ground state cooling of the Mg ion are explained and in Section 4 the experimental results on the cooling efficiency are discussed.

2 Setup

The following sections contain a detailed description of our experimental setup to employ Doppler and Raman resolved-sideband cooling of a $^{25}Mg^+$ ion stored in a linear Paul trap.

2.1 Solid-State Laser System for Magnesium

The Doppler cooling transition in $^{25}Mg^+$ is at a wavelength of 280 nm. We generate this light by frequency quadrupling a commercial fibre laser[1] at 1118.21 nm with a specified line width of < 70 kHz and an output power of 1 W, similarly to the setup presented in [22]. As

[1] Koheras Boostik^{TM}Y10/Menlo Systems GmbH orange one-1

shown in Figure 1, the output of the laser is frequency-doubled in a second-harmonic generation (SHG) bow-tie cavity by an anti-reflection-coated $4 \times 4 \times 18$ mm^3 Lithium Triborate (LBO) crystal[2] using 90° non-critical phase-matching of type I. A typical output power of $\sim$450 mW at 559 nm is observed after the cavity. Usually 15 mW of the output are picked up for frequency stabilizing the fibre laser using saturation spectroscopy in a molecular $^{129}I_2$ cell.

The output of the LBO cavity is coupled into a second bow-tie cavity which contains a $3 \times 3 \times 10$ mm^3 brewster-cut β-Barium-Borate (BBO) crystal[3] for SHG using critical phase-matching of type I. Here, a typical output power of $\sim$ 60 mW at 280 nm is observed. The length of each cavity is stabilized by the standard Hänsch-Couillaud locking technique [34].

The novelty in this setup consists of an electro-optical modulator[4] (EOM) that is located between the two doubling cavities to imprint sidebands at 9.2 GHz onto the green laser beam. The fibre laser is frequency-tuned such that one of the sidebands coincides with the $^2S_{1/2}$ to $^2P_{3/2}$ transition of $^{25}Mg^+$ which is used for Doppler cooling. The optical carrier, which is detuned by 9.2 GHz when sidebands are switched off, is employed for driving Raman transitions between two hyperfine states, as shown in Figure 4 and described in Section 2.3. This setup allows for fast switching between the resonant Doppler cooling and the off-resonant Raman configuration on a time scale faster than μs while using just a single laser system.

It is worthwhile mentioning that the imprinted sidebands are not frequency-doubled by the BBO cavity [20]. Since the EOM phase-modulates the electric field with frequency ω as

$$e^{i\omega t} \longrightarrow e^{i(\omega t + \beta \sin \Omega t)}, \qquad (1)$$

where β is the modulation index and $\Omega = 2\pi \times 9.2$ GHz, the BBO cavity only changes the modulation index by a factor of two

$$e^{i(\omega t + \beta \sin \Omega t)} \xrightarrow{\text{SHG}} e^{i(2\omega t + 2\beta \sin \Omega t)}.$$

The transmission of both $2\omega \pm \Omega$ sidebands through the BBO cavity is guaranteed by adjusting its free spectral range accordingly. The EOM is resonantly driven with a power of $\sim$2 W.

For the Raman configuration the laser beam is split into two branches. Each branch passes through an individual single-pass AOM which is resonantly driven at 450 MHz[5]. After that, the beams counter-propagate through the same AOM double-pass configuration (see Figure 2)

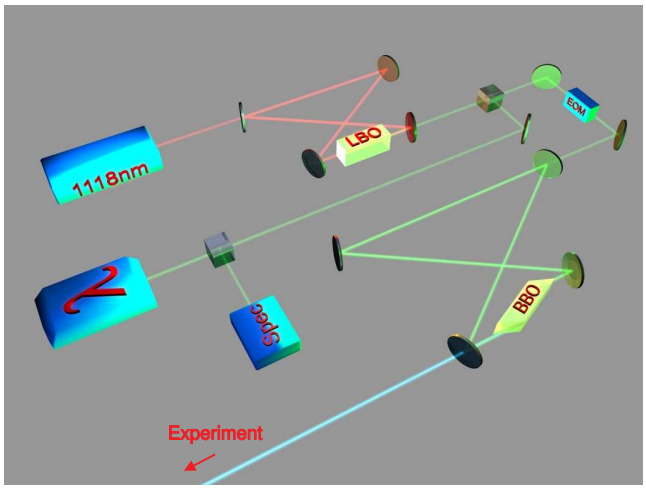

Fig. 1 Optical setup of the magnesium laser system. The output of a fibre laser at 1118 nm is frequency-quadrupled in two SHG cavities to drive transitions in $^{25}Mg^+$ ions (see text for details). Typically 15 mW of the green light is redirected to a saturated iodine spectroscopy (Spec) for frequency-locking of the fibre laser and a wavelength-meter for monitoring. An EOM imprints sidebands at 9.2 GHz on the green laser and allows for fast switching between a resonant Doppler cooling and an off-resonant Raman configuration.

consisting of two AOMs, driven at $\sim$220 MHz[6], providing two Raman laser beams (σ and π) with a frequency difference of 1.789 GHz. Typically, we achieve an efficiency of $\sim$70% for the single-pass AOMs and $\sim$50% for the double-pass AOMs for each branch.

This configuration, in contrast to otherwise used double-pass setups [23,24], has been chosen for two reasons. Firstly, the most common way to realize a double-pass AOM is by turning the linear polarization after the first pass of the AOM by 90° and then separating the overlapped retro-reflected beam from the incoming beam with a polarizing beam splitter . This is not possible in the ultra-violet (UV) since the diffraction efficiency of the UV grade fused silica crystal of the AOM strongly depends on the polarization. In a second approach, the beams are geometrically separated. This is usually done by a combination of a lens and a cat's eye which can for example be realized by two reflecting mirrors or a single right-angle prism. Using both these configurations in our setup, we have observed a degradation of the outgoing laser beam shape along with a significant decrease of the overall light transmission efficiency over a timescale of a few hours. We attribute this effect to UV-induced damage on the optical cathetus facet of the prism and on the mirror surfaces, respectively. Since a degradation was only observed on the first reflecting surfaces that were hit by the laser beam, we assume that the light intensity has to overcome a certain threshold to produce this effect [25]. In both cases, typically a $\sim$5 mW laser beam was focused to a waist of $50 - 70$ μm at the prism

[2] Castech Crystals Inc.
[3] Döhrer Elektrooptik
[4] Laser 2000 GmbH NFO-4851-M
[5] Brimrose Corp. QZF-450-100-.280
[6] IntraAction Corp. ASM-2202B3

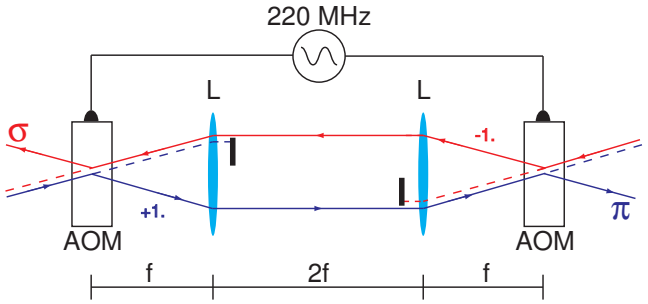

Fig. 2 Schematic of the double-pass AOM setup. The σ- and π-Raman beams are produced by two beams that counterpropagate. The 0^{th} order (dashed lines) of each AOM is blocked. The use of the lenses (L) allows for a frequency scan without shifting the outgoing beams. Both AOMs have to be supplied by the same frequency to fulfill the Bragg condition for each beam. The incoming and the outgoing overlapping beams are separated by translating them by a few mm (indicated by the small shift). This configuration avoids foci near optical surfaces.

or mirror, resulting in an intensity of $320-640$ kW/m^2. In order to circumvent this effect, we re-designed the double-pass AOM configuration, according to Figure 2, avoiding a focus near any of the optical surfaces.

The AOM setup provides the laser beams for off-resonant Raman excitation if the EOM is switched off. At the same time, the σ-Raman beam can be used to resonantly repump the population from the upper hyperfine manifold of the ground state (F=2) by switching on the EOM. This demonstrates the simplicity of this setup, since otherwise a second laser system providing an individual resonant repumping beam is necessary.

Our experimental sequences require pulsed operation, hence all laser beams are intensity stabilized by means of a sample-and-hold proportional-integral controller. A field-programmable gate array (FPGA) based pulse sequencer, which allows for frequency and phase-switching of six direct digital synthesis (DDS) output channels at a sub-μs rate [26], is used to provide frequency sources for all AOMs. Every time-critical component in the setup is referenced during all the measurements discussed here to a 10 MHz frequency standard[7].

2.2 Ion Trap

We produce $^{25}Mg^{+}$ ions using photoionization of a thermal beam of magnesium atoms provided by resistive-heating of a stainless-steel tube oven. A single light source at 285 nm with a power of $\sim$300 μW from a frequency-quadrupled diode laser is used for this process[8]. The diode laser has an output power of 100 mW and operates at a wavelength of 1140 nm. Its output is frequency-quadrupled by means of two cascaded SHG cavities, similar to the main laser setup[9].

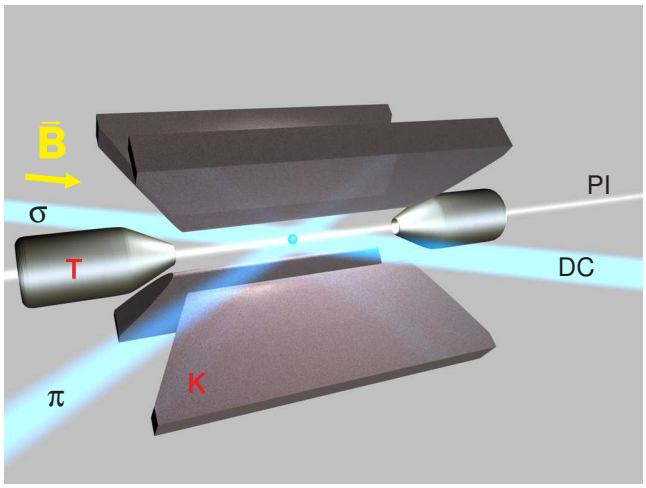

Fig. 3 Linear Paul trap. The trap consists of four blades (K) for radial confinement and two tip electrodes (T) for axial confinement. One pair of opposing blades is connected to a radio-frequency source at 23.81 MHz and the other pair is grounded. A DC voltage of 2 kV is applied to the tip electrodes. The distance between opposite blades is 1.6 mm, and that between the tips 5 mm. The photoionization laser at 285 nm (PI) is applied onto the ion through the tip electrodes. The Raman lasers (σ, π) are used in a crossed-configuration to provide an effective wave vector along the trap axis. The Doppler cooling beam (DC) is counterpropagating with the σ beam. A magnetic field of $\mathbf{B}\sim 0.6$ mT is co-aligned with the DC beam.

The atoms are ionized in a two-step process, involving the $^1P_1$ state in neutral magnesium. Although the natural abundance of the $^{25}Mg^{+}$ isotope is only $\sim$10%, it turns out to be sufficient for satisfactory loading rates of the desired isotope. The setup allows for isotope-selective loading by tuning the frequencies of the ionization and Doppler cooling lasers according to the isotope shifts [27].

After the ionization process, a single $^{25}Mg^{+}$ ion is stored in a linear Paul trap [28], as shown in Figure 3. Axial confinement is provided by applying a DC voltage of typically 2 kV to the tip electrodes and radial confinement is realized by applying a radio-frequency of 7 W at 23.81 MHz, which is then resonantly enhanced by means of a helical resonator [29], yielding an amplitude on the order of a few hundreds of volts at the radial blades. These parameters result in axial and radial harmonic confinement with trapping frequencies for $^{25}Mg^{+}$ of $(\omega_{\text{ax}}, \omega_{\text{rad}}) \sim 2\pi \times (1.9, 2.3)$ MHz.

[7] Stanford Research Systems DS-345
[8] Toptica DL pro
[9] In this case, the cavities contain a $LiNbO_3$ · MgO doped crystal (HG Photonics) and a BBO crystal (Castech Crystals Inc.) for SHG. Both cavities are stabilized using the Pound-Drever Hall locking technique [35].

2.3 State Initialization and Coherent Manipulation

The transitions used for cooling and coherent manipulation of the states of the ion are shown in the simplified level scheme of $^{25}Mg^{+}$ in Figure 4. During all measurements the degeneracy between the magnetic sub-levels is lifted by a magnetic field of $\mathbf{B} \sim 0.6$ mT. Doppler cooling of the ion is achieved by switching on the EOM sidebands, providing a near-resonant coupling of one of the sidebands to the $^2S_{1/2}$ to $^2P_{3/2}$ transition, which has a natural line width of $\gamma = 2\pi \times 41.4$ MHz [30].

To perform optimal cooling, the beam is detuned by half the line width by means of acousto-optical modulators (AOM). The beams polarization is carefully adjusted such that only σ^- ($\Delta m_F = +1$) transitions are addressed. While applying this beam, the ion is optically pumped into the $|\downarrow\rangle$ state, ideally leading to a closed cycling transition. Due to polarization imperfections, other magnetic sub-levels are excited, which decay into the $^2S_{1/2}$ (F=2) manifold during this process, so that a repumping beam (see below) is additionally applied during Doppler cooling to further improve state initialization.

For coherent manipulation of the ion, we couple the hyperfine ground states, $|\downarrow\rangle$ and $|\uparrow\rangle$, either by a Raman transition which is off-resonant by 9.2 GHz to the $^2S_{1/2}$ to $^2P_{3/2}$ transition or by direct application of radio-frequency at 1.789 GHz, corresponding to the hyperfine splitting in $^{25}Mg^{+}$ [31]. Sufficiently strong field gradients at the position of the ion are achieved by using an impedance-matched quarter-wave antenna made of a special coaxial cable[10] with an attenuation of 0.27 dB/m at 1.8 GHz. The antenna is attached to the outside of the vacuum chamber (see Figure 5) at a distance of $\sim$12 cm from the ion.

2.4 Fluorescence and State Detection

The fluorescence of the ion resulting from the excitation of the resonant Doppler cooling beam is collected by both a UV objective and an aluminum parabolic mirror (see Figure 5) and imaged onto a single photon counting module[11] (PMT) for quantitative readout. The fluorescence light can also be directed onto a CCD camera[12] to observe a geometrical image of the ion for alignment purposes. The UV objective is an extension of an existing design [32] covering a simulated solid-angle of $\sim 3-4\%$ of 4π, whereas the parabolic mirror[13] covers an angle of $\sim$11% for fluorescence collection [33]. Typically, a count rate of $\sim$240 kHz is observed from a single $^{25}Mg^{+}$ ion during Doppler cooling, when the laser is red-detuned by $\sim$20 MHz from the $^2S_{1/2}$ to $^2P_{3/2}$ transition.

[10] Andrew CommScope FSJ1-50A
[11] Hamamatsu Photonics H8259 MOD with R7518P
[12] Andor Technology iXon^{EM}+ 885 EMCCD
[13] Kugler Precision GmbH, custom-made

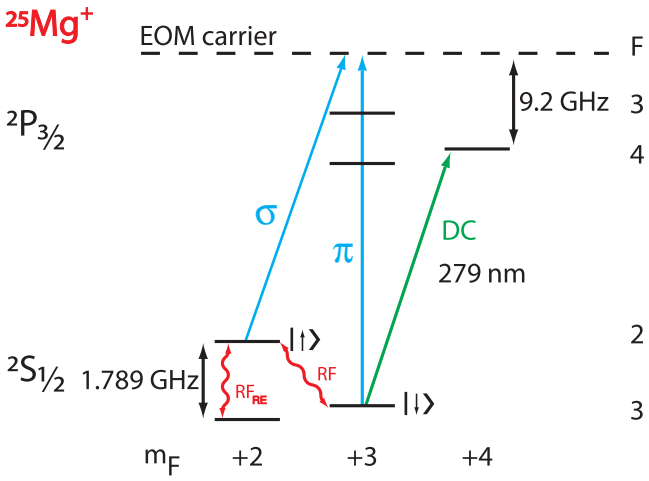

Fig. 4 Partial $^{25}Mg^{+}$ Level Scheme. The laser is tuned 9.2 GHz off-resonant with respect to the $^2S_{1/2}$ to $^2P_{3/2}$ transition. The optical carrier is used to drive coherent Raman transitions between the $|\downarrow\rangle := |F = 3, m_F = 3\rangle$ and $|\uparrow\rangle := |2, 2\rangle$ states by the σ- and π-Raman beams. Optical sidebands induced by an EOM are employed for resonant Doppler cooling on the cycling transition between the $^2S_{1/2}$ $|3, 3\rangle$ and $^2P_{3/2}$ $|4, 4\rangle$ states (DC beam). Magnetic field induced hyperfine transitions are driven by applying radio-frequency pulses at 1.789 GHz (RF and RF_{RE}).

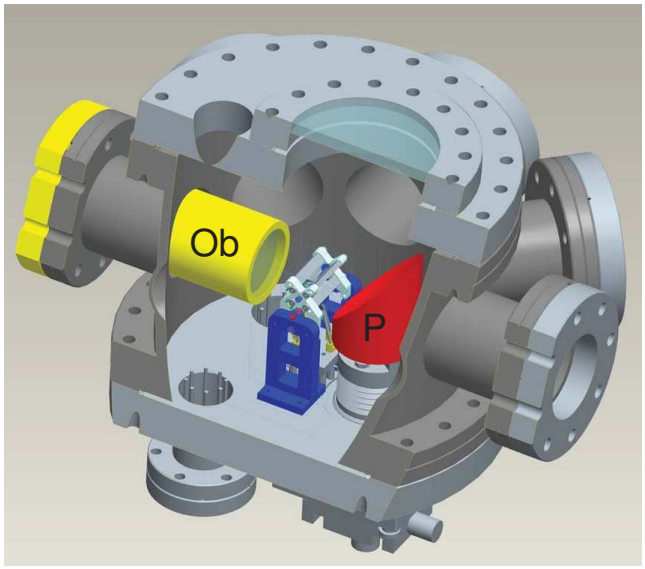

Fig. 5 Schematic cross-section of the vacuum setup. Fluorescence from the ion stored in the Paul trap (center) is collected via a UV objective (Ob) and a parabolic mirror (P). The objective is mounted inside an inverted viewport to minimize the distance to the ion for higher collection efficiency. Both channels are focused outside the vacuum chamber onto a PMT.

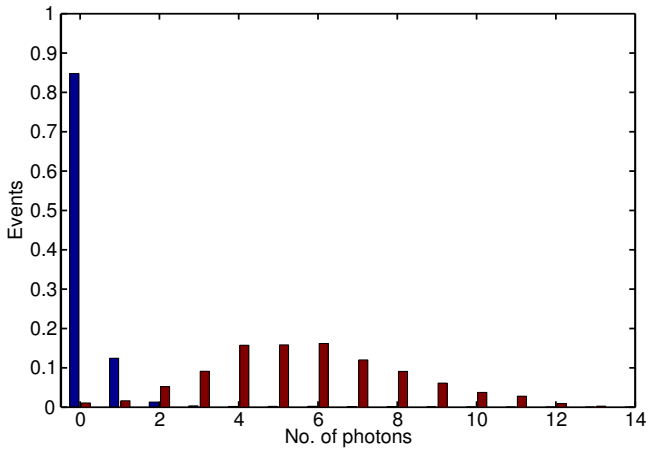

Fig. 6 Dark and bright state histograms. Typical calibrated histograms of the collected number of photons for a dark ion (blue bars), where only stray light is detected, and for a bright ion (red bars), where the ion is Doppler cooled and prepared in the $|\downarrow\rangle$ state. The average number of photons in this case is 0.2 and 5.8, respectively, for a 12.5 μs exposure time.

In all measurements described below, the ion is first initialized in the $|\downarrow\rangle$ state by applying the Doppler cooling and repumping laser beams for ~ 1 ms and then coherently manipulated according to the specific experimental sequence of laser pulses. After that, state detection is achieved via electron-shelving by applying the resonant Doppler cooling beam for typically $\sim$10–15 μs and counting the number of detected photons. In contrast to electron-shelving schemes in other ion species [14,19], the detection pulse is strongly restricted in length since the ion can be off-resonantly depumped from the $|\uparrow\rangle$ state, thus imitating a bright ion which was initially dark. Given this limitation, we typically detect a mean number of ~ 5.8 photons for a bright ion, whereas we observe a mean number of ~ 0.2 photons if the ion was dark.

The actual state amplitude a of the ion is determined by repeating the experiment $100-300$ times and fitting the resulting photon number distribution to previously calibrated, independent model distributions $\psi = a\psi_{\downarrow} + (1-a)\psi_{\uparrow}$, as shown in Figure 6. The distribution $\psi_{\uparrow}$ for a dark ion is recorded by switching off the EOM sidebands during the detection process, thus only accounting for stray light on the PMT, whereas the distribution $\psi_{\downarrow}$ for a bright ion is taken while the ion is Doppler cooled and prepared in the $|\downarrow\rangle$. Due to the rather low number of detected photons, both distributions are not orthogonal, resulting in an overlap integral of $\sum \psi_{\downarrow}\psi_{\uparrow} \sim 1.4\%$, which limits the single-shot readout fidelity.

2.5 Radio-Frequency Rabi Oscillations

As an initial measurement, we observe Rabi oscillations between two hyperfine ground states of $^{25}Mg^{+}$. In Figure 7 the probability of finding the Doppler cooled ion in the $|\uparrow\rangle$ state after subjecting it to a radio-frequency pulse at 1.789 GHz is shown as a function of the pulse duration. Applying the calibrated state detection procedure, we observe the expected sinusoidal state evolution with a Rabi frequency of $\Omega_{\mathrm{RF}} = 2\pi \times 63.74(7)$ kHz and a contrast of $97.8 \pm 1.4\%$.

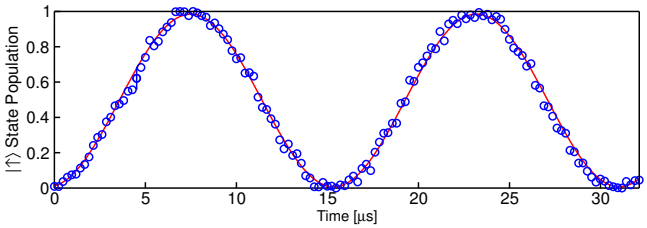

Fig. 7 Radio-frequency induced Rabi oscillations between the $|\downarrow\rangle$ and the $|\uparrow\rangle$ state. Each point corresponds to 300 measurements. The average error resulting from the dark and bright state distribution fit is on the order of $\pm 3\%$ for each point and is omitted in the graph for clarity. A sinusoidal fit (solid red line) yields a Rabi frequency of $\Omega_{\mathrm{RF}} = 2\pi \times 63.74(7)$ kHz and a contrast of $97.8 \pm 1.4\%$ for the oscillation.

It is worth mentioning that the motion of the ion can be neglected in this measurement, since the Lamb-Dicke criterion is fulfilled for the radio-frequency transition [19].

3 Ground State Cooling

After Doppler cooling, the $^{25}Mg^{+}$ ion reaches a thermal state with a temperature of $T_{\mathrm{DC}} \sim 1$ mK [36]. This corresponds to a mean vibrational population number of the harmonic trapping potential $\bar{n} \sim 10$, with a trapping frequency of $\omega_T \sim 2\pi \times 2$ MHz. The population distribution for these parameters is depicted in Figure 8.

We further cool a single ion in axial direction via Raman sideband cooling [15] by applying first and second order red sideband ($1^{\mathrm{st}}/2^{\mathrm{nd}}$ RSB) pulses which couple the internal (electronic) with the external (vibrational) degrees of freedom. This is accomplished by detuning both Raman beams by one or two trapping frequencies and adjusting the pulse duration for each target state according to the calculated Rabi frequencies in Figure 8 [19]. Reinitialization and dissipation is achieved by applying a resonant repump laser pulse using the σ-polarized Raman beam with the EOM switched on. From the excited state, the ion can decay into the target state ($|\downarrow\rangle$), but also into the $|3,2\rangle$ state. This population is recovered by applying a radio-frequency π-pulse between the $|3,2\rangle$ and $|2,2\rangle$ states ($\mathrm{RF}_{\mathrm{RE}}$), followed by another optical repump pulse. Repeating this sequence several times, the atomic population is reinitialized into the $|\downarrow\rangle$ state. Each RSB pulse-repump sequence removes one quantum of motion from the ion in the trap, until the ground state is achieved.

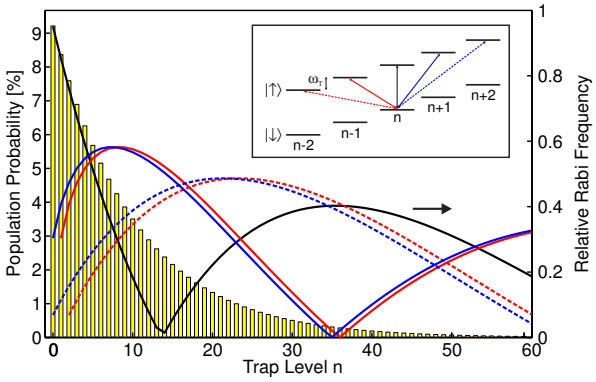

Fig. 8 Population distribution and Rabi frequencies. The bar graph (yellow) shows the population distribution for a $^{25}Mg^{+}$ at the Doppler cooling limit (1 mK) in a 1D harmonic potential with a trapping frequency of $\omega_T = 2\pi \times 2$ MHz. In addition, the functional dependence of the Rabi frequencies of the carrier (black line), 1st red (blue) sideband (red (blue) solid lines) and 2nd red (blue) sideband (dashed lines) are shown for a Lamb-Dicke factor of $\eta = 0.32$ as a function of the initial n-state. The inset schematically depicts the different transitions (same color coding) for the effective two-level system in the harmonic trap.

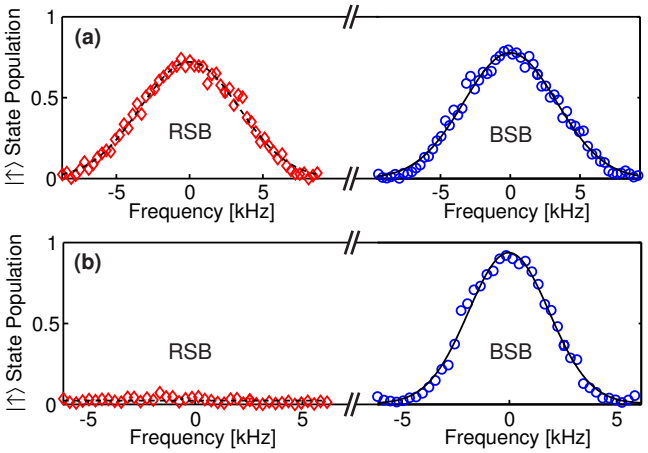

Fig. 9 Sideband excitations. Frequency scans over the 1st red and blue sidebands (diamonds and circles) for a Doppler cooled **(a)** and a sideband cooled **(b)** $^{25}Mg^{+}$ ion are shown. The missing excitation on the red sideband clearly indicates the high ground state occupancy. The frequencies are shifted for clarity. The average error resulting from the dark and bright state distribution fit is on the order of $\pm 3\%$ for each point and is omitted in the graph for clarity. The solid (dashed) lines correspond to Gaussian fits of the red (blue) sideband resonance.

The complete sideband cooling sequence begins with a series of $25\times$ 2nd RSB pulses, starting from $n_{ax} \sim 40$, which are followed by $15\times$ 1st RSB pulses, starting from $n_{ax} \sim 15$, to cool the ion to the ground state. Each set of pulses is usually repeated $2-3$ times to improve the cooling process. The use of the 2nd RSB in this procedure is necessary, since ion population in n-levels beyond the zero crossing of the Rabi frequency of the 1st RSB cannot be efficiently transferred below this point using only the 1st RSB. The total sideband cooling sequence typically takes $\sim 10-15$ ms.

4 Results

Figure 9 shows the measured excitation on both RSB and BSB resonances for a Doppler cooled and an axially sideband cooled single $^{25}Mg^{+}$ ion, respectively. As the ground state is expected to be a dark state for the red sidebands, the 1st RSB shows no excitation after sideband cooling, whereas the 1st BSB excitation rises almost to unity. The ratio $Q = \rho_R/\rho_B$ of the RSB (ρ_R) and BSB (ρ_B) excitations gives the average axial vibrational population $\bar{n}_{ax}$ [37]

$$\bar{n}_{ax} = \frac{Q}{1-Q}, \qquad (2)$$

as well as the population in the axial ground state $P(n = 0) = 1 - Q$. The analysis of the observed resonances, along with Rabi oscillations on the sidebands, yields an $\bar{n}_{ax} = 0.03 \pm 0.01$ as an upper limit for the mean occupancy. This corresponds to a ground state population of $P(n = 0) \sim 97\%$.

The fact that the ion is predominantly in a single state after sideband cooling also manifests itself in a significant difference in the observed Rabi oscillations on the Raman carrier transitions. These transitions do not change the motional quantum number, nevertheless their Rabi frequency depends on the motion, as shown in Figure 8. In case the ion is Doppler cooled, an average over many oscillations with different Rabi frequencies is given, whereas if the ion occupies a Fock state, an oscillation with a single frequency is expected. This behavior is clearly shown in the observed Raman-stimulated Rabi oscillations on the carrier transition, as depicted in Figure 10. We attribute the observed decay of the oscillation for the sideband cooled ion to several effects: dephasing due to residual $n > 0$ population, magnetic field and intensity fluctuations and loss of coherence due to off-resonant excitation from the Raman beams. This last effect has been calibrated to increase (decrease) the ion excitation by $\sim 0.02\%/\mu$s ($\sim 0.06\%/\mu$s) for an ion in the $|\downarrow\rangle$ ($|\uparrow\rangle$) state to first order. Taking this into account, the analysis of the ground state population yields $\bar{n}_{ax} = 0.02 \pm 0.01$.

It should be noted, that off-resonant excitation could be significantly reduced by operating the system at an optical carrier detuning of 18.4 GHz and using the 2nd order EOM sidebands for cooling or by employing an EOM with a higher resonance frequency.

5 Conclusion

In summary, we have demonstrated ground state cooling of a single trapped $^{25}Mg^{+}$ ion employing a frequency-

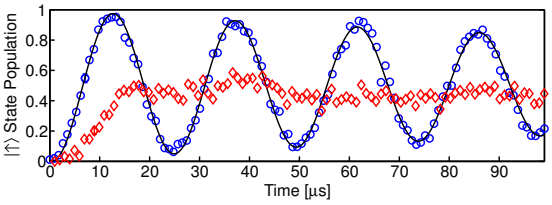

Fig. 10 Raman-stimulated Rabi oscillations on the carrier transition for a Doppler cooled (diamonds) and a sideband cooled (circles) $^{25}Mg^{+}$ ion. The thermal average over many Rabi frequency components results in a flat line for an excitation time beyond $15\mu s$ in case of the Doppler cooled ion, whereas for the sideband-cooled ion a single-frequency oscillation is observed. The average error resulting from the dark and bright state distribution fit is on the order of $\pm 3\%$ for each point and is omitted in the graph for clarity. The solid line corresponds to an exponentially decaying sinusoidal, yielding a Rabi frequency of $\Omega = 2\pi \times 40.9(1)$ kHz and a decay rate of $\Gamma = 4.2(4) \times 10^3 s^{-1}$.

quadrupled commercial fibre laser system. An EOM in the laser system allows for fast switching between a resonant cooling/repumping configuration and an off-resonant Raman laser configuration, respectively. This is a cost-effective simplification to other solid-state laser setups for Mg^{+} ions [22]. The performance of the laser system was demonstrated in a pulsed ground state cooling experiment with results comparable to the best achieved with more complex laser systems.

A further simplification of the optical setup can be achieved if only ground-state cooling is required. In this case, RSB pulses can be applied between two Zeeman components of the ground state of an ion without hyperfine structure, such as $^{24}Mg^{+}$, eliminating the need to bridge the hyperfine structure with AOMs. The demonstrated system can be used for a large variety of experiments involving ground-state cooling and coherent manipulation of ions.

Acknowledgements We would like to thank Rainer Blatt for generous loan of equipment and support. We thank Uwe Sterr for providing the iodine spectroscopy cell. We further acknowledge the technical support of S. Haslwanter, A. Schönherr, H. Jordan, M. Kluibenschädl, A. Wander, P.-C. Carstens and G. Hendl. We gratefully acknowledge financial support by the Austrian START program of the Austrian Ministry of Education and Science, the Cluster of Excellence QUEST, Hannover, and the Physikalisch-Technische Bundesanstalt, Braunschweig.

References

1. R. Blatt and D. Wineland, Entangled states of trapped atomic ions. Nature **453**, 1008 (2008)
2. J. I. Cirac and P. Zoller, Quantum computations with cold trapped ions. Phys. Rev. Lett. **74**, 4091 (1995)
3. C. W. Chou, D. B. Hume, J. C. J. Koelemeij, D. J. Wineland, and T. Rosenband, Frequency Comparison of Two High-Accuracy Al^{+} Optical Clocks. Phys. Rev. Lett. **104**, 070802 (2010)
4. T. Rosenband, D. B. Hume, P. O. Schmidt, C. W. Chou, A. Brusch, L. Lorini, W. H. Oskay, R. E. Drullinger, T. M. Fortier, J. E. Stalnaker, S. A. Diddams, W. C. Swann, N. R. Newbury, W. M. Itano, D. J. Wineland, J. C. Bergquist, Frequency ratio of Al^{+} and Hg^{+} single-ion optical clocks; Metrology at the 17th decimal place. Science **319**, 1808 (2008)
5. P. O. Schmidt, T. Rosenband, C. Langer, W. M. Itano, J. C. Bergquist, and D. J. Wineland, Spectroscopy using quantum logic. Science **309**, 749 (2005)
6. C. F. Roos, M. Chwalla, K. Kim, M. Riebe and R. Blatt, 'Designer atoms' for quantum metrology. Nature **443**, 316 (2006)
7. A. L. Wolf, S. A. van den Berg, W. Ubachs and K. S. E. Eikema, Direct frequency comb spectroscopy of trapped ions. Phys. Rev. Lett. **102**, 223901 (2009)
8. A. Friedenauer, H. Schmitz, J. Glueckert, D. Porras and T. Schaetz, Simulating a quantum magnet with trapped ions. Nature Physics **4**, 757 (2008)
9. R. Gerritsma, G. Kirchmair, F. Zähringer, E. Solano, R. Blatt and C. F. Roos, Quantum simulation of the Dirac equation. Nature **463**, 68 (2010)
10. W. Paul, Electromagnetic traps for charged and neutral particles. Rev. Mod. Phys. **62**, 531540 (1990)
11. H. Häffner, F. Schmidt-Kaler, W. Hänsel, C. F. Roos, T. Körber, M. Chwalla, M. Riebe, J. Benhelm, U. D. Rapol, C. Becher, R. Blatt, Robust entanglement. Appl. Phys. B **81**, 151 (2005)
12. C. Langer, R. Ozeri, J. D. Jost, J. Chiaverini, B. DeMarco, A. Ben-Kish, R. B. Blakestad, J. Britton, D. B. Hume, W. M. Itano, D. Leibfried, R. Reichle, T. Rosenband, T. Schaetz, P. O. Schmidt, and D. J. Wineland, Long-Lived Qubit Memory Using Atomic Ions. Phys. Rev. Lett. **95**, 060502 (2005)
13. J. Eschner, G. Morigi, F. Schmidt-Kaler and R. Blatt, Laser cooling of trapped ions. J. Opt. Soc. Am. B **20** 1003 (2003)
14. D. Leibfried, R. Blatt, C. Monroe, D. J. Wineland, Quantum dynamics of single trapped ions. Rev. Mod. Phys. **75**, 281 (2003)
15. C. Monroe, D. M. Meekhof, B. E. King, S. R. Jefferts, W. M. Itano and D. J. Wineland, P. Gould, Resolved-sideband raman cooling of a bound atom to the 3D zero-point energy. Phys. Rev. Lett. **75**, 4011 (1995)
16. T. Schneider, B. Roth, H. Duncker, I. Ernsting and S. Schiller, All-optical preparation of molecular ions in the rovibrational ground state. Nature Physics **6**, 275 (2010)
17. Peter F. Staanum, Klaus Højbjerre, Peter S. Skyt, Anders K. Hansen and Michael Drewsen, Rotational laser cooling of vibrationally and translationally cold molecular ions. Nature Physics **6**, 271 (2010)
18. G. Kirchmair, J. Benhelm, F. Zähringer, R. Gerritsma, C. F. Roos and R. Blatt, High-fidelity entanglement of ions of $^{43}Ca^{+}$ hyperfine clock states. Phys. Rev. A **79**, 020304 (2009)
19. D. J. Wineland, C. Monroe, W. M. Itano, D. Leibfried, B. E. King, D. M. Meekhof, Experimental issues in coherent quantum-state manipulation of trapped atomic ions. J. Res. Natl. Inst. Stand. Technol. **103**, 259 (1998)
20. P. J. Lee, B. B. Blinov, K. Brickman, L. Deslauriers, M. J. Madsen, R. Miller, D. L. Moehring, D. Stick, and C.

Monroe, Atomic qubit manipulations with an electro-optic modulator. Optics Letters **28**, 1582 (2003)
21. S. Olmschenk, K. C. Younge, D. L. Moehring, D. Matsukevich, P. Maunz, and C. Monroe, Manipulation and detection of a trapped Yb^+ hyperfine qubit. Phys. Rev. A **76**, 052314 (2007)
22. A. Friedenauer, F. Markert, H. Schmitz, L. Petersen, S. Kahra, M. Herrmann, Th. Udem, T. W. Hänsch and T. Schaetz, High power all solid state laser system near 280 nm. Applied Physics B **84**, 371 (2006)
23. C.-H. Chang, R. K. Heilmann, M. L. Schattenburg, and P. Glenn, Design of a double-pass shear mode acousto-optic modulator. Rev. of Sci. Instr. **79**, 033104 (2008)
24. E. A. Donley, T. P. Heavner, F. Levi, M. O. Tataw, and S. R. Jefferts, Double-pass acousto-optic modulator system. Rev. of Sci. Instr. **76**, 063112 (2005)
25. R. A. Negres, M. A. Norton, D. A. Cross, C. W. Carr, Growth behavior of laser-induced damage on fused silica optics under UV, ns laser irradiation. Optics Express **18**, 19966 (2010)
26. P. Pham, A general-purpose pulse sequencer for quantum computing. Master's thesis, Massachusetts Institute of Technology (2005)
27. E. J. Salumbides, S. Hannemann, K. S. E. Eikema, W. Ubachs, Isotopically resolved calibration of the 285-nm Mg I resonance line for comparison with quasar absorptions. Mon. Not. R. Astron. Soc. **373**, L41L44 (2006)
28. S. Gulde, Experimental realization of quantum gates and the Deutsch-Josza algorithm with trapped $^{40}Ca^+$-ions. Ph.D. Thesis, University of Innsbruck (2003)
29. W. W. Macalpine and R. O. Schildknecht, Coaxial resonators with helical inner conductor. Proc. IRE, 2099–2105 (1959)
30. Ralchenko, Yu., Kramida, A.E., Reader, J. and NIST ASD Team (2008). NIST Atomic Spectra Database (version 4.0), [Online]. Available: http://physics.nist.gov/asd3 [Monday, 25-Oct-2010 07:53:09 EDT]. National Institute of Standards and Technology, Gaithersburg, MD.
31. W. M. Itano and D. J. Wineland, Precision measurement of the ground-state hyperfine constant of $^{25}Mg^+$. Phys. Rev. A **24**, 1364 (1981)
32. W. Alt, An objective lens for efficient fluorescence detection of single atoms. Optik **113**, 142144 (2002)
33. A detailed manuscript is in preparation.
34. T. W. Hänsch and B. Couillaud, Laser frequency stabilization by polarization a spectroscopy of a reflecting reference cavity. Opt. Commun. **35**, 441 (1980)
35. R. W. P. Drever, J. L. Hall, F. V. Kowalski, J. Hough, G. M. Ford, A. J. Munley, H. Ward, Laser phase and frequency stabilization using an optical resonator. Appl. Phys. B **31**, 97 (1983)
36. D. J. Wineland and W. M. Itano, Laser cooling of atoms. Phys. Rev. A **20**, 1521 (1979)
37. Q. A. Turchette, D. Kielpinski, B. E. King, D. Leibfried, D. M. Meekhof, C. J. Myatt, M. A. Rowe, C. A. Sackett,C. S. Wood, W. M. Itano, C. Monroe, and D. J. Wineland, Heating of trapped ions from the quantum ground state. Phys. Rev. A **61**, 063418 (2000)